Diffusion-limited aggregation on curved surfaces

2010 EPL 91 46005

(http://iopscience.iop.org/0295-5075/91/4/46005)

A Letters Journal Exploring the Frontiers of Physics

August 2010

EPL, **91** (2010) 46005
doi: 10.1209/0295-5075/91/46005

www.epljournal.org

Diffusion-limited aggregation on curved surfaces

J. Choi[1], D. Crowdy[2] and M. Z. Bazant[1,3(a)]

[1] *Department of Mathematics, Massachusetts Institute of Technology - Cambridge, MA 02139, USA*
[2] *Department of Mathematics, Imperial College - London, UK, EU*
[3] *Department of Chemical Engineering, Massachusetts Institute of Technology - Cambridge, MA 02139, USA*

received 4 May 2010; accepted in final form 10 August 2010
published online 15 September 2010

PACS 61.43.Hv – Fractals; macroscopic aggregates (including diffusion-limited aggregates)
PACS 47.54.-r – Pattern selection; pattern formation
PACS 89.75.Kd – Patterns

Abstract – We develop a general theory of transport-limited aggregation phenomena occurring on curved surfaces, based on stochastic iterated conformal maps and conformal projections to the complex plane. To illustrate the theory, we use stereographic projections to simulate diffusion-limited aggregation (DLA) on surfaces of constant Gaussian curvature, including the sphere ($K > 0$) and the pseudo-sphere ($K < 0$), which approximate "bumps" and "saddles" in smooth surfaces, respectively. Although the curvature affects the global morphology of the aggregates, the fractal dimension (in the curved metric) is remarkably insensitive to curvature, as long as the particle size is much smaller than the radius of curvature. We conjecture that all aggregates grown by conformally invariant transport on curved surfaces have the same fractal dimension as DLA in the plane. Our simulations suggest, however, that the multifractal dimensions increase from hyperbolic ($K < 0$) to elliptic ($K > 0$) geometry, which we attribute to curvature-dependent screening of tip branching.

Introduction. – The Laplacian growth model and its stochastic analogue, diffusion-limited aggregation (DLA) [1], describe the essential physics of non-equilibrium pattern formation in diverse situations [2]. Examples include viscous fingering [3], dendrite solidification [4], dielectric breakdown [5], and dissolution [6], depending on conditions at the moving, free boundary. Some extensions to non-Laplacian growth phenomena, such as advection-diffusion-limited aggregation [7,8] (ADLA) and brittle fracture [9], are also available, which exploit mathematical similarities with the DLA model.

Almost all prior work with these growth models has assumed flat Euclidean space, typically a two-dimensional plane, but real aggregates, such as mineral dendrites [10], cell colonies [11], and cancerous tumors [12], often grow on curved or rough surfaces. In principle, surface curvature should affect the morphology of stochastic aggregates, but we are not aware of any prior work, except for simulations of Eden-like clusters on spheres [11], which lack the long-range interactions of DLA and related models through the evolving concentration field. In the case of continuous interfacial motion, there have been several mathematical studies of viscous fingering (without surface tension) on spheres [13,14], but we will show that stochastic aggregation of discrete particles is rather different, due to the physical constraint of fixed particle size in the curved space.

In this letter, we extend transport-limited growth models to curved two-dimensional surfaces via conformal projections from the plane. Time-dependent conformal maps are widely used in physics [15] and materials science [16] to describe interfacial dynamics in two dimensions. Continuous conformal maps have long been applied to viscous fingering [3,17], and more recently, Hastings and Levitov introduced stochastic, iterated conformal maps for DLA [18]. Both continuous and stochastic conformal-map dynamics have also been extended to other conformally invariant (but non-Laplacian and nonlinear) gradient-driven transport processes [7,8,19], such as advection-diffusion in a potential flow [20,21] or electrochemical transport in a quasi-neutral solution [19]. Indeed, there is nothing special about harmonic functions (solutions to Laplace's equation) in the plane, aside from the direct connection to analytic functions of a complex variable (real or imaginary part). The key property of conformal invariance is shared by other

(a) E-mail: bazant@mit.edu

equations [16,19] and, as noted here, applies equally well to conformal (*i.e.* angle preserving) transformations between curved surfaces. We formulate continuous and discrete conformal-map dynamics for surfaces of constant Gaussian curvature, not only the sphere with positive curvature, but also the pseudosphere, with negative curvature. We use the approach to study the fractal and multi-fractal properties of DLA on curved surfaces.

Transport-limited growth on curved surfaces. – At first, it would seem that conformal-map dynamics cannot be directly applied to a non-Euclidean geometry, and certainly the formulation could not be based only upon analytic functions of the complex plane. Nevertheless, if there exists a conformal (angle-preserving) map between the curved manifold and the plane, and if the underlying transport process is conformally invariant [7,8,16,19,21], then any solution to the transport equations in the non-Euclidean geometry can be conformally mapped to a solution in the complex plane, without changing its functional form. Such maps do exist, as we illustrate below with important special cases.

Let $\Omega_m(t)$ be the exterior of a growing object on a non-Euclidean manifold, M, and Φ be a conformal map from a (part of) complex plane to M. We speak of the domain $\Omega_m(t)$ as having its *shadow*, $\Omega_z(t) = \Phi^{-1}(\Omega_m(t))$, on the complex plane under the *projection* Φ^{-1}. As in the flat-surface case, we can describe the growth by a time-dependent conformal map, $g(w,t)$, from the exterior of the unit disk, Ω_w, to the exterior of the growing shadow, $\Omega_z(t)$, which in turn is mapped onto the curved geometry by the inverse projection. Care must only be taken that the dynamics of $g(w,t)$ should describe $\Omega_z(t)$ in such a way that the evolving object, $\Omega_m(t)$, follows the correct physics of growth on M, rather than in the intermediate complex plane, which is purely a mathematical construct. In particular, to model the stochastic aggregation of identical particles of fixed size in the curved space M, the particle size must vary with position in the shadow domain, due to local stretching by the conformal map to the plane.

Let us illustrate this point for both continuous and discrete versions of conformally invariant, transport-limited growth [8,16]. For continuous growth, we generalize the Polubarinova-Galin equation equation [8,16,22] for a curved manifold with a conformal map $\Phi(z)$ as follows:

$$\mathrm{Re}\left\{\overline{w\ g'(w)}\ g_t(w)\right\} = \frac{\alpha\,\sigma(w,\,t)}{|\Phi' \circ g(w)|^2}. \qquad (1)$$

for $|w| = 1$, where α is a constant and $\sigma(w,\,t)$ is the time-dependent flux density on the boundary of Ω_w. This result is easily obtained by substituting $\Phi \circ g$ for g in the original equation.

For stochastic growth, we adjust the Hastings-Levitov algorithm [18] on the shadow domain. The algorithm is based on the recursive updates of the map,

$$g_n(w) = g_{n-1} \circ \phi_{\lambda_n,\theta_n}(w), \quad g_n(w) = g(w,t_n), \qquad (2)$$

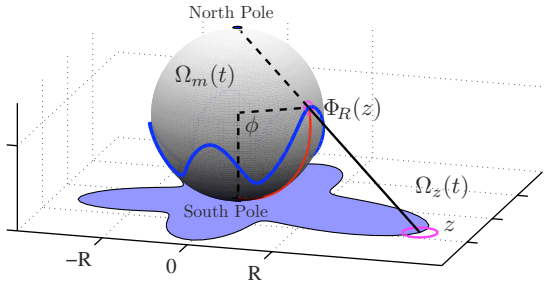

Fig. 1: (Colour on-line) Stereographic projection, Φ^{-1}, from the exterior of the growing object $\Omega_m(t)$ on a sphere of radius R to the exterior of the shadow, $\Omega_z(t)$, on a complex plane. The point $\Phi(z)$ is projected from the north pole to the point z. The origin of the z-plane is tangent to the sphere at the south pole, and the latitudinal angle ϕ is measured from the south pole.

where $\phi_{\lambda,\theta}$ is a specific map that slightly distort Ω_w by a bump of area λ around the angle θ. While the random sequence $\{\theta_n\}$ follows the probability distribution, $p(\theta, t_n) \propto \sigma(e^{i\theta}, t_n)$, invariant under conformal maps, the preimage of bump area, λ_n, should be determined so that the bump area is fixed as λ_0 on the manifold, M. Thus the bump size of the n-th accretion is determined by

$$\lambda_n = \frac{\lambda_0}{|\Phi' \circ g_{n-1}(e^{i\theta_n})|^2 \cdot |g'_{n-1}(e^{i\theta_n})|^2}. \qquad (3)$$

We are not aware of any prior modification of the Hastings-Levitov algorithm with this general form. Previous studies on DLA in a channel geometry [23] could be viewed as the case $M = \{z : 0 < \arg z < 2\pi\}$ and $\Phi(z) = \log(z)$, although the manifold is Euclidean.

It is important to stress that our general transport-limited growth models are not conformally invariant in the most general sense, since the full *time-evolution of the interface* cannot be simply mapped from one geometry to another. It is only the growth probability measure for stochastic dynamics (or the interfacial velocity distribution for continuous dynamics) *for a particular realization of the interface, at a given moment in time*, which is invariant under conformal mapping. In the case of DLA in curved geometries (discussed below), this means that the angles on the unit disk in the complex plane (the pre-image of the cluster in curved space, after inverting the projection and the iterated Hastings-Levitov map in the plane) are independent, identically distributed random variables, but the particle size must vary in the complex plane, to maintain a constant size after projection to the curved space.

Stereographic projections. – To illustrate the general theory, we first make use of the classical stereographic projection [24,25] to describe growth on a (Riemann) sphere. A stereographic projection is obtained by projecting the surface of a sphere from the north pole to a plane whose origin is tangent to the south pole; see fig. 1. If Φ is an *inverse* stereographic projection

with sphere of radius R, Φ^{-1} maps the point (R,ϕ,θ) in spherical coordinates to $z = R\tan(\phi/2)e^{i\theta}$ in the complex plane. Here θ is the azimuthal angle and ϕ is the latitudinal angle measured from the south pole. If the modulus, $|\cdot|$, on the sphere is defined to be the distance to the origin (south pole) in the curved metric (arc-length of the great circle) in a similar way to $|\cdot|$ on a complex plane, $|z|$ and $|\Phi(z)|$ satisfy

$$\frac{|z|}{2R} = \tan\left(\frac{|\Phi(z)|}{2R}\right). \tag{4}$$

The Jacobian factor of the projection is angle-independent; thus, it is given by

$$|\Phi'(z)| = \frac{\mathrm{d}|\Phi(z)|}{\mathrm{d}|z|} = \frac{1}{1+(|z|/2R)^2} \tag{5}$$

from the derivative of eq. (4). Using eq. (5), we can formulate continuous interfacial dynamics, eq. (1), or stochastic dynamics, eq. (3) on a sphere.

While the surface of a sphere is a three-dimensional visualization of an elliptic (or Riemannian) geometry with constant positive Gaussian curvature $K = R^{-2}$, there also exists a conformal projection to the complex plane from a hyperbolic geometry with constant negative curvature, $K = -R^{-2}$. Physically, the hyperpolic geometry locally resembles a saddle point, or "mountain pass", on a curved surface. Unlike an elliptic geometry, a hyperbolic geometry cannot be isometrically embedded in 3D Euclidean space. (In other words, it is not possible for a surface in three dimensions to consist entirely of saddle points.) Instead, only a part of the geometry can be embedded in three dimensions, through a surface known as the *pseudosphere*. A conformal projection to the complex plane can be obtained by simply viewing the hyperbolic geometry as a surface of a sphere with an imaginary radius, iR, as suggested from the sign of curvature. Substituting iR for R alters eqs. (4) as

$$\frac{|z|}{2R} = \tanh\left(\frac{|\Phi(z)|}{2R}\right) \tag{6}$$

and eq. (5) as

$$|\Phi'(z)| = \frac{1}{1-(|z|/2R)^2}. \tag{7}$$

The image of hyperbolic geometry under the projection is thus limited to the interior of a disk with radius $2R$, and the boundary, $|z| = 2R$, corresponds to the infinity. The stereographic projection serves as a non-isometric visualization of the geometry known as *Poincaré disk*. The length element $\mathrm{d}z$ at $\mathrm{d}z$ in the planar disk corresponds to the element $\mathrm{d}z/(1-(|z|/2R)^2)$ in the hyperbolic geometry.

DLA on constant-curvature surfaces. – We now illustrate our general mathematical formalism by simulating DLA clusters in geometries of constant curvature, where the (fixed) particle size is much smaller than the radius of curvature. This allows to grow large clusters (*e.g.* without hitting the opposite pole of the sphere) and consider universal effects of surface curvature, which do not depend on the particle size. As discussed above, the harmonic probability measure on the disk in the plane, $p(\theta) = 1/2\pi$, is equivalent to the physical growth probability measure on the cluster in the curved geometry, obtained by iterated conformal maps in the plane, eq. (3), followed by stereographic projection to the curved geometry.

Representative DLA clusters grown by our method are shown in fig. 2, for both elliptic and hyperbolic geometries. The former is represented in fig. 2(a) by a cluster of equal-sized particles growing on a sphere from the south pole, towards a particle source at the north pole. Since it is impossible to embed the latter in three dimensions, we show instead the "shadow" of the cluster in the Poincaré disk, $|z| < 2R$, where the particles shrink in size with distance from the origin. In both cases, the spatial variation of the particle sizes in the shadow domain (to keep constant particle size in the curved physical domain) yields subtle differences in cluster morphology, compared to the familiar case of DLA clusters in a Euclidean geometry.

A significant advantage of the conformal-mapping formulation of DLA, compared to discrete random-walk simulations, is that the Laurent expansion of $g(w,t)$ analytically encodes information about the geometrical moments of the cluster [18,26]. For example, the *conformal radius*, A_1, and the *center of charge*, A_0, come from the first two terms of the expansion, $g(w) \approx A_1 w + A_0$. Such coefficients obtained from DLA clusters on curved surfaces are not directly useful, however, since they are the moments of the mathematical shadow in the complex plane, not the original cluster in the physical domain. Nevertheless, using the property that circles are mapped to circles under an (inverse) stereographic projection, it is possible to define analogous quantities corresponding to A_1 and A_0.

We note that the image, $\Phi(A_1 w + A_0)$, of the unit circle, $|w| = 1$, is also a circle on M, and it is the one that best approximates the cluster and the far-field in $\Omega_m(t)$. Thus, we define the conformal radius, $\mathcal{A}_1$, and the center of charge, $\mathcal{A}_0$, on M to be the radius and the deviation of $\Phi(A_1 w + A_0)$ respectively:

$$\mathcal{A}_1 = \frac{1}{2}\left\{\,|\Phi(A_1 + |A_0|)| + |\Phi(A_1 - |A_0|)|\,\right\}, \tag{8}$$

$$\mathcal{A}_0 = \frac{1}{2}\left\{\,|\Phi(A_1 + |A_0|)| - |\,\Phi(A_1 - |A_0|)|\,\right\}. \tag{9}$$

On curved surfaces, however, the fractal dimension D_f, cannot be determined from the scaling, $n \sim \langle \mathcal{A}_1 \rangle^{D_f}$, since the geometry is not linearly scalable with $\mathcal{A}_1$; the two domains within radii of different values of $\mathcal{A}_1$ are not self-similar to each other, and the log-log plot of n *vs.* $\mathcal{A}_1$ is not linear either.

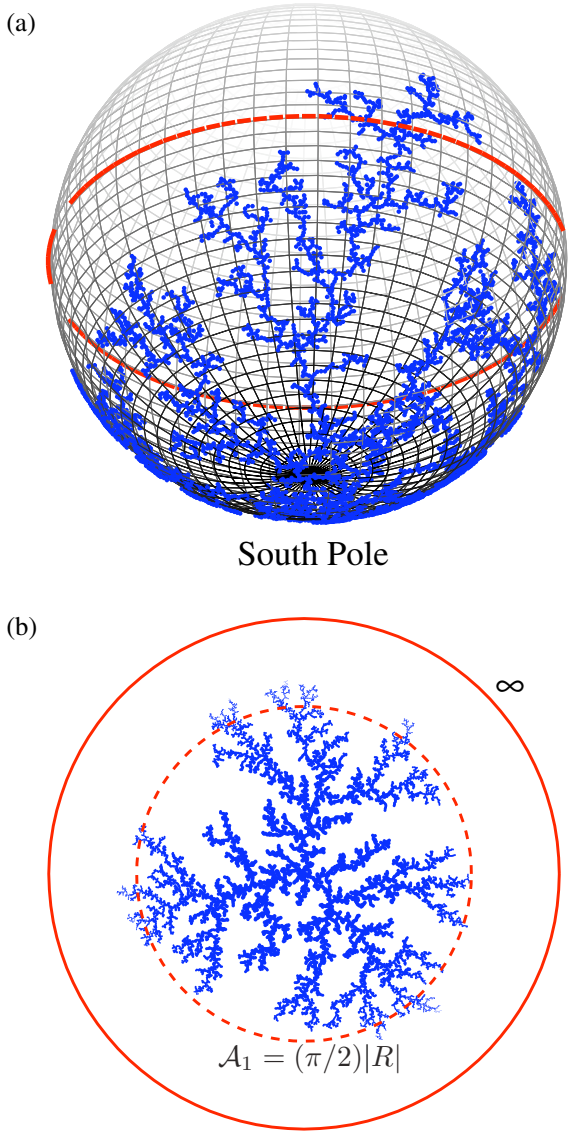

Fig. 2: (Colour on-line) DLA clusters on the elliptic (a) and the hyperbolic (b) geometries. The elliptic geometry is isometrically embedded on the surface of a sphere and the hyperbolic geometry is visualized on the Poincaré disk with the metric, $\mathrm{d}s = \mathrm{d}z/(1-(|z|/2R)^2)$. We use $R/\sqrt{\lambda_0} = 100$ and aggregate 4942 and 9001 particles to fill the great circles of radius $(\pi/2)R$ (dashed lines) in the elliptic and hyperbolic geometries, respectively.

Table 1: The fractal dimension D_f and the multifractal dimensions D_{2q+1} of DLA clusters on three different geometries.

Geometry	Elliptic	Euclidean	Hyperbolic
D_f	1.704 ± 0.001	1.704 ± 0.001	1.693 ± 0.001
D_2/D_f	0.577 ± 0.003	0.529 ± 0.006	0.527 ± 0.001
D_3/D_f	0.591 ± 0.006	0.503 ± 0.005	0.499 ± 0.001
D_4/D_f	0.617 ± 0.012	0.486 ± 0.004	0.482 ± 0.001
D_5/D_f	0.631 ± 0.018	0.473 ± 0.004	0.469 ± 0.001

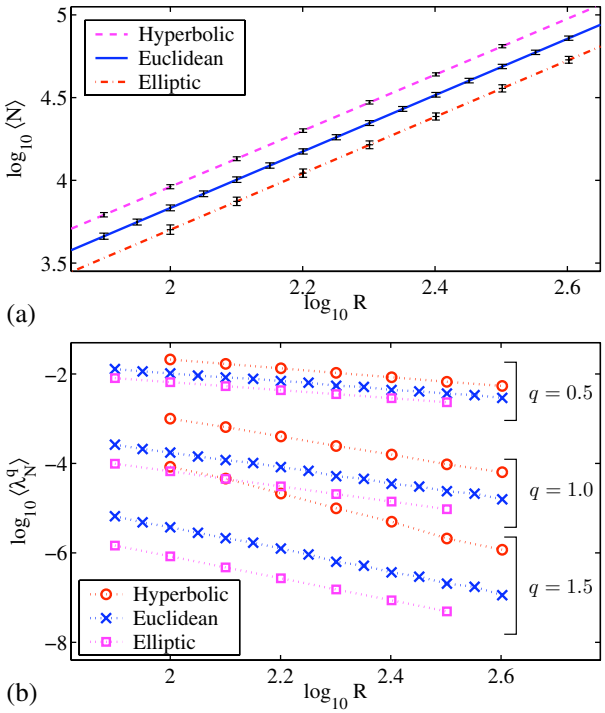

Fig. 3: (Colour on-line) (a) The average number of particles, $\langle N \rangle$, to fill the disk of conformal radius, $\mathcal{A}_1 = (\pi/2)R$, *vs.* radius R on the three geometries. (b) Moments $\langle \lambda_N^q \rangle$ of the pre-image bump size, λ_N, *vs.* R, which define D_{2q+1} via (10).

Instead, we study the fractal properties of the clusters as follows. We use the sphere radius R as a relevant length scale while keeping $\mathcal{A}_1$ proportional to R for self-similarity. Thus, we grow a cluster until $\mathcal{A}_1$ reaches $\phi_0 R$ for various radiuses R, but with a fixed particle size, $\lambda_0 = 1$, and a fixed angle $\phi_0 = \pi/2$. The angle ϕ_0 is as such since the circle (dashed lines in fig. 2) becomes a great circle on a sphere. If N is the number of particles to fill the radius, the fractal dimension is determined from $\langle N \rangle \sim R^{D_f}$. From the statistics of 1000 clusters for each R in a geometrically increasing sequence from 79 to 400, we obtain the fractal dimensions, $D_f \approx 1.70$, as shown in table 1. Figure 3(a) shows $\langle N \rangle$ *vs.* R in the three geometries. The relative deviation of D_f between geometries is surprisingly small compared to the deviation of the surface properties caused by the curvature. For example, the area contained within a radius $(\pi/2)R$ in the elliptic (or hyperbolic) geometry is about 23% smaller (or larger) than the corresponding area in the Euclidean space. Nevertheless, this factor only changes the prefactor, not the exponent, of the scaling, $\langle N \rangle \sim R^{D_f}$.

Our results suggest that the fractal dimension D_f is insensitive to the surface curvature. This property is apparently related to the fact that, over small length scales comparable to the the particle size $\sqrt{\lambda_0}$, the surface is locally Euclidean. This result is consistent with previous studies of ADLA clusters [8], whose fractal dimension

is unaffected by the background flow of concentrated fluid, even though the flow strongly influences the global morphology and "mean shape" of the clusters [7]. We conjecture that *any conformally invariant transport-limited aggregation process on a d-dimensional curved manifold has same, universal fractal dimension as DLA in flat (Euclidean) space in d dimensions*. This includes complicated stochastic phenomena, such as ADLA growth of aggregates in a two-dimensional fluid flow on the surface a sphere or pseudosphere (hyperbolic saddle).

More subtle statistics of the aggregates, related to the warping of particle sizes by projections from curved geometries to the plane, are revealed by multifractal scalings. The multifractal properties [27,28] of the clusters, which derive from time-evolution of the probability measure, do seem to depend on the curvature in our simulations. Following ref. [26], we measure the multifractal dimensions D_q from the relation,

$$\langle \lambda_N^q \rangle \sim R^{-2qD_{2q+1}}. \tag{10}$$

The averaging in eq. (10) is made over λ_N at uniformly distributed angle. Figure 3(b) shows the first three moments of λ_N as functions of R, and table 1 shows D_q/D_f in the three geometries. We note that D_q for the elliptic geometry seem to be still transient, influenced by finite-size effects. The multifractal dimensions do not satisfy the inequality $D_q > D_{q'}$ for $q < q'$ [27]. Since the space itself is finite and the distance to *infinity* is bounded, the instability in growth is pronounced in elliptic geometry. The normalized center-of-charge fluctuation, $\langle |\mathcal{A}_0|^2 \rangle^{1/2}/R$, is about 0.3 for an elliptic geometry although it decreases as R increases. For Euclidean and hyperbolic geometries, the fluctuations are around 0.03 and 0.02, respectively. It should also be noted that the growth probability on the sphere is not the usual harmonic measure since the far-field potential, $-\log|z|$, on plane is mapped to the singular potential, $\log(\pi - \phi)$, around the north pole.

In spite of some lingering finite-size effects in our simulation results, we conjecture that multifractal dimensions increase in the order of hyperbolic, Euclidean, and elliptic geometries. The justification is that, when the measurements are similarly made for decreasing latitudinal angles, $\phi_0 = \pi/3$ and $\pi/6$, D_q on elliptic and hyperbolic geometries, they converge to D_q on the Euclidean plane. This is also supported by the slight difference in D_q between Euclidean and hyperbolic geometries, which does not appear to be attributable to statistical error.

Although we have not performed a detailed analysis of the cluster morphologies corresponding to different multifractal exponents, we believe the observed dependence of D_q on curvature is related to the depth of "fjords" between growing branches of clusters grown in the different geometries. In elliptic geometry, the circumference of a circle with radius $\phi_0 R$ is $2\pi \sin \phi_0 R$, which is shorter than $2\pi\phi_0 R$ in Euclidean geometry. This has fundamental implications for "screening" by the tips of neighboring branches of a growing cluster, which preferentially attach particles before they can penetrate deep into the fjord between the branches. If we consider a pair of branches which make the same opening angle on the two geometries, the area between them is more screened in elliptic geometry than in Euclidean geometry. Therefore, we expect a different distribution of λ due to the different spatial curvature. Due to the competition neighboring regions on a smaller circumference, tip-splitting events are subdued, as observed in continuous growth [14], and eventually fewer branches survive. Although we have not performed a detailed analysis of tip splitting, some evidence for this effect can be seen in fig. 2(b), where the DLA cluster seems to become less branched at larger radii. The opposite argument applies to hyperbolic geometry, where the circumference is given by $2\pi \sinh \phi_0 R$, the inter-branch area is less screened, and tip splitting is encouraged. Effectively, there is more space for branches to split and grow separately in the hyperbolic geometry, which can be seen qualitatively in fig. 2(b), where the cluster becomes increasingly more branched at larger radii. In future work, it would be interesting to analyze the spectrum of λ and its connection to tip splitting events.

In summary, we have developed a mathematical theory of transport-limited growth on curved surfaces and applied it to DLA on two-dimensional surfaces of constant Gaussian curvature. Our simulations suggest that the fractal dimension of DLA clusters is universal, independent of curvature, and depends only on the spatial dimension. The multifractal properties of DLA, however, seem to depend on curvature, since tip-splitting is related to the different degrees of screening of the inter-branch areas. We conjecture that these results hold in general, for any conformally invariant transport-limited growth process, in any number of dimensions.

* * *

We acknowledge helpful discussions with E. Somfai.

REFERENCES

[1] Witten T. A. and Sander L. M., *Phys. Rev. Lett.*, **47** (1981) 1400.
[2] Bunde A. and Havlin S. (Editors), *Fractals and Disordered Systems,* second edition (Springer, New York) 1996.
[3] Bensimon D., Kadanoff L., Shraiman B. I. and Tang C., *Rev. Mod. Phys.*, **58** (1986) 977.
[4] Kessler D. A., Koplik J. and Levine H., *Adv. Phys.*, **37** (1988) 255.
[5] Niemeyer L., Pietronero L. and Wiesmann H. J., *Phys. Rev. Lett.*, **52** (1984) 1033.
[6] Bazant M. Z., *Phys. Rev. E*, **73** (2006) 060601.
[7] Davidovitch B., Choi J. and Bazant M. Z., *Phys. Rev. Lett.*, **95** (2005) 075504.

[8] Bazant M. Z., Choi J. and Davidovitch B., *Phys. Rev. Lett.*, **91** (2003) 045503.
[9] Barra F., Levermann A. and Procaccia I., *Phys. Rev. E*, **66** (2002) 066122.
[10] Chopard B., Herrmann H. J. and Vicsek T., *Nature*, **353** (1991) 409.
[11] Wang C. Y. and Bassingthwaighte J. B., *Math. Biosci.*, **142** (1997) 91.
[12] Ho P. F. and Wang C. Y., *Math. Biosci.*, **155** (1999) 139.
[13] Entov V. M. and Etingof P. I., *Eur. J. Appl. Math.*, **8** (1997) 23.
[14] Parisio F., Moraes F., Miranda J. A. and Widom M., *Phys. Rev. E*, **63** (2001) 036307.
[15] Gruzberg I. and Kadanoff L. P., *J. Stat. Phys.*, **114** (2004) 1183.
[16] Bazant M. Z. and Crowdy D., in *Handbook of Materials Modeling*, edited by Yip S. *et al.*, Vol. **I** (Springer) 2005, Art. 4.10.
[17] Howsion S. D., *Eur. J. Appl. Math.*, **3** (1992) 209.
[18] Hastings M. and Levitov L., *Physica D*, **116** (1998) 244.
[19] Bazant M. Z., *Proc. R. Soc. A.*, **460** (2004) 1433.
[20] Kornev K. and Mukhamadullina G., *Proc. R. Soc. London, Ser. A*, **447** (1994) 281.
[21] Choi J., Margetis D., Squires T. M. and Bazant M. Z., *J. Fluid Mech.*, **536** (2005) 155.
[22] Polubarinova-Kochina P. Ya., *Dokl. Akad. Nauk SSSR*, **47** (1945) 254; Galin L. A., *Dokl. Akad. Nauk SSSR*, **47** (1945) 246.
[23] Somfai E., Ball R. C., DeVita J. P. and Sander L. M., *Phys. Rev. E*, **68** (2003) 020401.
[24] Needham T., *Visual Complex Analysis* (Oxford University Press) 1997.
[25] Jones G. A. and Singerman D., *Complex Functions: An Algebraic Geometric Viewpoint* (Cambridge University Press) 1987.
[26] Davidovitch B., Hentschel H. G. E., Olami Z., Procaccia I., Sander L. M. and Somfai E., *Phys. Rev. E*, **59** (1999) 1368.
[27] Hentschel H. G. E. and Procaccia I., *Physica D*, **8** (1983) 435.
[28] Halsey T. C., Jensen M. H., Kadanoff L. P., Procaccia I. and Shraiman S., *Phys. Rev. A*, **33** (1986) 1141.